Traveling-wave Uni-Traveling Carrier Photodiodes for continuous wave THz generation

Efthymios Rouvalis[1], Cyril C. Renaud[1], David G. Moodie[2], Michael J. Robertson[2] and Alwyn J. Seeds[1*]

[1]*UCL Electronic and Electrical Engineering, Torrington Place, London WC1E 7JE, UK*
[2]*Centre for Integrated Photonics, Adastral Park, Ipswich IP5 3RE, UK*
**a.seeds@ee.ucl.ac.uk*

Abstract: The design, experimental evaluation and performance of a Traveling-Wave Uni-Traveling Carrier photodiode for Terahertz generation are described and its advantages in terms of frequency response are demonstrated. The device delivered 148 μW at 457 GHz, 24 μW at 914 GHz when integrated with resonant antennas and 105 μW at 255 GHz, 30 μW at 408 GHz, 16 μW at 510 GHz and 10 μW at 612 GHz. Record levels of Terahertz figure of merit (P_{THz}/P_{opt}^2 in W^{-1}) were achieved ranging from 1 W^{-1} at 110 GHz to 0.0024 W^{-1} at 914 GHz.

OCIS codes: (250.0250) Optoelectronics; (040.5160) Photodetectors; (230.7020) Traveling-wave devices.

References and links

1. P. H. Siegel, "Terahertz Technology," IEEE Trans. Microw. Theory Tech. **50**(3), 910–928 (2002).
2. B. Ferguson, and X. C. Zhang, "Materials for terahertz science and technology," Nat. Mater. **1**(1), 26–33 (2002).
3. H. Eisele, A. Rydberg, and G. I. Haddad, "Recent advances in the performance of InP Gunn devices and GaAs TUNNETT diodes for the 100-300-GHz frequency range and above," IEEE Trans. Microw. Theory Tech. **48**(4), 626–631 (2000).
4. H. Eisele, "Third-Harmonic Power Extraction from InP Gunn Devices up to 455 GHz," IEEE Microw. Wirel. Compon. Lett. **19**(6), 416–418 (2009).
5. H. Eisele, "355 GHz oscillator with GaAs TUNNETT diode," Electron. Lett. **41**(6), 329 (2005).
6. M. Ino, T. Ishibashi, and M. Ohmori, "CW oscillation with p+-p-n+ silicon IMPATT diodes in 200 GHz and 300 GHz bands," Electron. Lett. **12**(6), 148–149 (1976).
7. G. Chattopadhyay, E. Schlecht, J. Gill, S. Martin, A. Maestrini, D. Pukala, F. Maiwald, and I. Mehdi, "A Broadband 800 GHz Schottky Balanced Doubler," IEEE Microw. Wirel. Compon. Lett. **12**(4), 117–118 (2002).
8. E. R. Brown, K. A. McIntosh, K. B. Nichols, and C. L. Dennis, "Photomixing up to 3.8 THz in low-temperature-grown GaAs," Appl. Phys. Lett. **66**(3), 285 (1995).
9. A. Wade, G. Fedorov, D. Smirnov, S. Kumar, B. S. Williams, Q. Hu, and J. L. Reno, "Magnetic-field-assisted terahertz quantum cascade laser operating up to 225 K," Nat. Photonics **3**(1), 41–45 (2009).
10. M. A. Belkin, F. Capasso, F. Xie, A. Belyanin, M. Fischer, A. Wittmann, and J. Faist, "Room temperature terahertz quantum cascade laser source based on intracavity difference-frequency generation," Appl. Phys. Lett. **92**(20), 201101–201103 (2008).
11. C. C. Renaud, M. Robertson, D. Rogers, R. Firth, P. J. Cannard, R. Moore, and A. J. Seeds, "A high responsivity, broadband waveguide uni-traveling carrier photodiode," Proc. SPIE **6194**, 61940C–61940C–8 (2006).
12. K. S. Giboney, J. W. Rodwell, and J. E. Bowers, "Traveling-wave photodetector theory," IEEE Trans. Microw. Theory Tech. **45**(8), 1310–1319 (1997).
13. H. Ito, S. Kodama, Y. Muramoto, T. Furuta, T. Nagatsuma, and T. Ishibashi, "High-speed and high-output InP-InGaAs unitraveling-carrier photodiodes," IEEE J. Sel. Top. Quantum Electron. **10**(4), 709–727 (2004).
14. J. Campbell, S. Demiguel, and N. Li, "High-speed photodetectors," *31st European Conference on Optical Communication* (Glasgow, Scotland, 2005), pp. 493–496 vol.3.
15. F. Xia, J. K. Thomson, M. R. Gokhale, P. V. Studenkov, J. Wei, W. Lin, and S. R. Forrest, "An asymmetric twin-waveguide high-bandwidth photodiode using a lateral taper coupler," IEEE Photon. Technol. Lett. **13**(8), 845–847 (2001).
16. A. J. Seeds, F. Pozzi, C. C. Renaud, M. J. Fice, L. Ponnampalam, D. C. Rogers, I. F. Lealman, and R. Gwilliam, "Microwave Photonics: Opportunities for Photonic Integration", *14th European Conference on Integrated Optics* (Eindhoven, The Netherlands, 2008), Th1, pp. 123–132.
17. C. C. Renaud, D. Moodie, M. Robertson, and A. J. Seeds, "High Output Power at 110 GHz with a Waveguide Uni-Travelling Carrier photodiode," *The 20th Annual Meeting of the IEEE Lasers and Electro-Optics Society* (Lake Buena Vista, Florida, USA, 2007), pp. 782–783.

#126657 - $15.00 USD Received 7 Apr 2010; revised 29 Apr 2010; accepted 29 Apr 2010; published 11 May 2010

18. E. A. Michael, "Travelling-wave photonic mixers for increased continuous-wave power beyond 1 THz," Semicond. Sci. Technol. **20**(7), S164–S177 (2005).
19. D. Lasaosa, J. W. Shi, D. Pasquariello, K. G. Gan, M. C. Tien, H. H. Chang, S. W. Chu, C. K. Sun, Y. J. Chiu, and J. E. Bowers, "Traveling-Wave Photodetectors with High Power-Bandwidth and Gain-Bandwidth Product Performance," IEEE J. Sel. Top. Quantum Electron. **10**(4), 728–741 (2004).

1. Introduction

The exploitation of frequencies located in the Terahertz (THz) part of the spectrum (100 GHz to 10 THz), the region between microwaves and far-infra-red, is expected to offer a variety of applications [1]. For example, a plethora of materials can be identified by their rotational and vibrational responses lying in this spectral range [2]. Additionally, numerous applications can be found in communications technology, security, imaging, biology and medicine. However, development of technology for this part of the electromagnetic spectrum has been limited due to the absence of compact sources that can operate efficiently at these frequencies. Significant work in millimetre-wave range solid-state sources has shown output power levels of the order of mW [3]. In the submillimeter-wave range, sources based on InP-based Gunn diodes have achieved 283 μW at 412 GHz and 23 μW at 455 GHz [4], more than 140 μW at 355 GHz from Tunnel injection Transit-Time (TUNNETT) diodes [5] and 200 μW at 361 GHz from a room-temperature Impact Avalanche Transit-Time (IMPATT) diode [6]. A common method to overcome the frequency limitations of solid-state oscillator sources is their integration with frequency multipliers, with those based on planar Schottky diodes producing power levels of 1 mW at 775 GHz [7]. Other common solutions for generating THz power include photomixing in Low-Temperature Grown GaAs [8]. The highest THz power ever demonstrated from room-temperature photomixing in photoconductors up to 1 THz being of the order of 1 μW [8]. Quantum Cascade Lasers (QCL) can offer sub-THz signals when magnetic field assisted [9], but only 300 nW output power for room temperature operation at 5 THz [10]. Optical Heterodyne Generation (OHG) in wide bandwidth photodiodes appears to be a promising technique for realising a room temperature THz source [11]. Key advantages stemming from OHG are wide tuning range and high spectral purity. Such a THz source utilises ultra-fast photodetectors and the performance of the source depends on the high-frequency response of the photodetector [11]. Bandwidth limitations in a conventional p-i-n structure are imposed by the carrier transit time as well as the load resistance and the intrinsic and parasitic capacitances. The Traveling-Wave Photodiode (TW-PD) [12] and the Uni-Traveling Carrier Photodiode (UTC-PD) [13] are two separate photodetection structures that have already been independently demonstrated, with improved performance compared to conventional p-i-n devices. In this article, we describe the development of a waveguide-fed, Traveling-Wave Uni-Traveling Carrier photodiode (TW-UTC-PD) [11]. First, the operating principles of the device are discussed and its expected performance compared with other photodiodes. Subsequently, the devices and the experimental techniques for their evaluation are described. Finally, the waveguide-fed TW-UTC-PD, integrated with different types of antennas is demonstrated as an integrated, tuneable THz source. In this paper we demonstrate narrow-band output powers of 148 μW at 457 GHz and 24 μW at 914 GHz for devices integrated with resonant antennas with P_{opt} = 100 mW and 105 μW at 255 GHz down to 10 μW at 612 GHz for devices integrated with broadband antennas with P_{opt} = 40 mW. To the best of our knowledge, the TW-UTC-PD showed the highest THz figure of merit (P_{THz}/P_{opt}^2 in W^{-1}) yet reported in this frequency range from a photomixing source.

2. Theoretical analysis, design and simulation results

In $In_{1-x}Ga_xAs_{1-y}P_y$ quaternary semiconductor materials and under low field conditions, the electron drift velocity is considerably higher than that for holes. In a typical UTC-PD structure [13] the processes of light absorption and carrier collection are separated. In this case, where the absorber is p-doped, holes are majority carriers and respond within the relaxation time, whereas electrons diffuse towards the depletion layer. The photocurrent in the depletion layer is dominated by the overshoot velocity of electrons and the total transit time depends on the fast electron transport across the absorption and depletion layers, increasing the transit time

#126657 - $15.00 USD Received 7 Apr 2010; revised 29 Apr 2010; accepted 29 Apr 2010; published 11 May 2010

limited cut-off frequency substantially relative to conventional photodiodes. In a TW-PD with an open input termination the RC bandwidth limitation is replaced with the TW-PD limitation that depends on the optical absorption coefficient and the mismatches between the optical and the forward and backward traveling waves as defined in [12]. While the p-i-n TW-PD structure is capable of high responsivities with a waveguide-fed design, saturation effects can lead to limited output power. Combining the TW-PD structure with the UTC-PD active layer design can obviate this limitation. However, the coupling of the optical signal to a waveguide photodiode is challenging. One of the most effective techniques to improve the coupling efficiency to the device is the use of a secondary, non-absorbing, InGaAsP waveguide adjacent to the carrier collection layer [14].

By careful design of the layer structure, the optical signal distribution can be enhanced as the absorption can be distributed over the length of the device, resulting in reduced space-charge effects and allowing for yet higher levels of output power and substantially improved DC responsivity values. The length where 90% of the optical power is absorbed was used as a design parameter to define the length of the device. Using this coupling rule as the starting point, two different types of ridge guide devices were fabricated (Fig. 1), one employing an absorber of 120 nm (type 1) and the other a thinner absorber of 70 nm (type 2) chosen to improve the transit time.

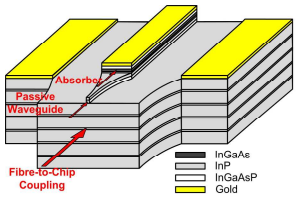

Epitaxial Structure

Doping	Material	Function	Thickness (nm)
Zn (>2E18)	p-Q1.3	Barrier & p-contact	200
Zn (1.5E18)	p-InGaAs	Absorber	120 (type 1), 70 (type 2)
S (1E16)	n-Q1.3	Spacer	30
S (1E16)	n-InP	Depletion	300
S (1-2E18)	n-Q1.3	Waveguide	300
S (3-4E18)	n-InP	n-contact	700

Fig. 1. Schematic of the taper waveguide integrated device. Type 1 devices (120 nm absorber) were integrated with a passive waveguide. Type 2 devices (70 nm absorber) were integrated with an InP/InGaAsP diluted taper waveguide.

For the type 1 devices the length was designed to be 15 μm and the width of the ridge to be 4 μm. For the type 2 devices the lengths were 50 and 75 μm and the widths 2.5 and 3 μm. The device electrodes were designed to have a 50 Ω characteristic impedance. The type 2 devices were also integrated with an InP/InGaAsP diluted taper waveguide to improve the coupling efficiency from a fibre (Fig. 1) [15].

In order to depict the advantage arising from employing a traveling wave configuration, a vertically illuminated UTC-PD, a p-i-n TW-PD and a TW-UTC-PD (type 1) with the same capacitance, series resistance and inductance were modelled (Fig. 2).

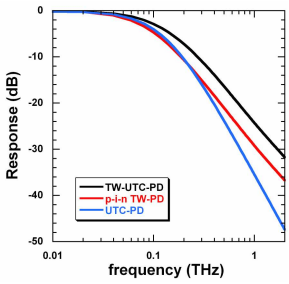

Fig. 2. Modelled frequency response up to 2 THz with 50 Ω load for a type 1, 4x15 μm^2 TW-UTC-PD (black) compared with a 4x15 μm^2 p-i-n TW-PD (red) and a 60 μm^2 area lumped UTC-PD (blue).

An equivalent Transmission Line model was developed for both TW devices and a lumped circuit model for the vertically illuminated device [12]. According to the modelling results, the advantage was calculated to be >10 dB_{elec} at 1 THz and >14 dB_{elec} at 2 THz for the TW-UTC-PD. A comparison with a p-i-n TW-PD shows an advantage of >5 dB_{elec} at the same

#126657 - $15.00 USD Received 7 Apr 2010; revised 29 Apr 2010; accepted 29 Apr 2010; published 11 May 2010

frequencies. The combination of the UTC and the TW photodetection structures in a single device with a diluted taper waveguide is therefore expected to give significantly improved performance in terms of output power for a given optical input power compared with other types of photodiodes.

3. Device realisation and testing

The photodetectors were fabricated on semi-insulating InP as described in [16]. Two separate configurations to extract high millimetre-wave and THz output power were employed. The first used a 150 μm spacing, coplanar waveguide to couple through a Ground-Signal-Ground probe into millimetre-wave coaxial cables and rectangular waveguides. The second configuration was developed to estimate the performance of the device in the THz frequency range and included both broadband and narrowband antennas to couple the THz output to free-space. Figure 3 shows SEM images of the photodetectors integrated with a coplanar waveguide (Fig. 3a), a Bow-Tie antenna (Fig. 3b), a Log-Periodic antenna (Fig. 3c) and a resonant antenna (Fig. 3d).

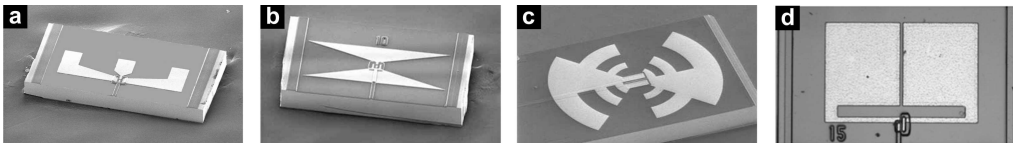

Fig. 3. SEM pictures of the different TW-UTC devices fabricated with: a) coplanar probe contacts (type 1 & 2), b) Bow-Tie antennas (type 2), c) Log-Periodic antennas (type 2), d) resonant antennas (type 1).

Three experimental configurations were used to assess photodetector performance, depending on the frequency range and device configuration. In the first, a Lightwave Component Analyser (LCA) was used to measure the detector frequency dependent photo-response up to 40 GHz.

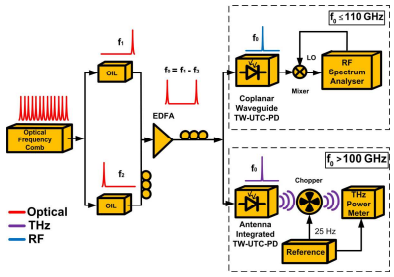

Fig. 4. Experimental arrangement for RF and THz measurements.

The second, used for measurements above 40 GHz, is shown in Fig. 4. For measurements over the frequency range of 40 GHz to 110 GHz, the measurement technique labelled in Fig. 4 as $f_0 \leq 110$ GHz was used. An heterodyne signal from two SG-DBR (Sampled Grating-Distributed Bragg Reflector) lasers Optically Injection Locked (OIL) to an Optical Frequency Comb Generator (OFCG) [11] was injected into the device. This system allows for the generation of high purity millimetre-wave and submillimeter-wave signals. For all measurements the input optical power to the photodiode was set to give a photocurrent of 10 mA. To measure the frequency response above 40 GHz with a spectrum analyser the probes were connected to different calibrated harmonic microwave mixers to measure the output power at the desired measurement frequency. Losses in this configuration were up to 45 dB_{elec} at 110 GHz (3 dB_{elec} from the probe and up to 42 dB_{elec} from the mixer) and a frequency dependent loss correction was included.

For measurements above 110 GHz the experimental arrangement labelled as $f_0 > 100$ GHz in Fig. 4 was used. Here photodiodes with integrated antennas were used and the THz power was measured using a Thomas Keating Power Meter with accuracy of 5 μW

#126657 - $15.00 USD Received 7 Apr 2010; revised 29 Apr 2010; accepted 29 Apr 2010; published 11 May 2010

which was operated within an homodyne chopping system at a frequency of 25 Hz in order to increase the Signal-to-Noise Ratio (SNR). The background power that did not correspond to the THz frequency domain (Blackbody Radiation, residual IR power from the device and ambient noise) was filtered with a polyethylene film. The signal-ASE heterodyne noise in the Erbium Doped Fibre Amplifier (EDFA) was also measured and extracted by pumping the device with one laser only at the same EDFA output power in order to generate the same signal-ASE noise level that corresponds to the amplified heterodyne signal. The calibration frequency of the power meter was kept constant and the final results were corrected to the power meter response afterwards to keep the measured level of noise constant.

4. Millimeter wave experimental results

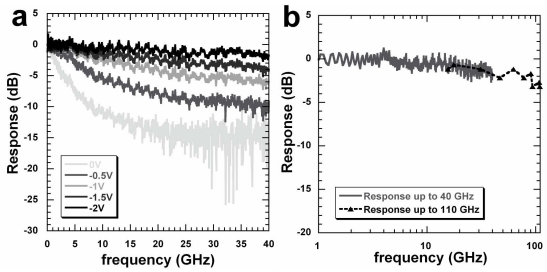

Fig. 5. (a) bias dependence up to 40 GHz (4x15 μm^2), (b) frequency response up to 110 GHz (4x15 μm^2).

Using the first experimental system, the bias dependent frequency response up to 40 GHz was measured for a 4x15 μm^2 type 1 device. The measurements, shown in Fig. 5a, demonstrate that, as expected, with 0V bias the −3 dB$_{elec}$ bandwidth was very low. At −1 V the bandwidth increased to 20 GHz and at −2 V the response was essentially flat up to 40 GHz. No further improvement in bandwidth was observed with a bias more negative than −2 V. Similar performance was obtained for the type 2 devices but the optimum bias point was found to be at −3.5V. Subsequently, to obtain the relative response of the photodetector up to 110 GHz the heterodyne system was employed. Additional measurements were taken for frequencies below 40 GHz to check the consistency of the heterodyne system results with LCA measurements. The results were compared to the LCA measurements and agreement to within 0.1 dB$_{elec}$ was observed. As seen in Fig. 5b, the response remains above −3dB$_{elec}$ up to 108.2 GHz within the measurement error. The DC responsivity of the devices ranged from 0.14 A/W for antenna integrated type 1 devices to 0.32 A/W for type 2 devices at a wavelength of 1.55 μm, with no DC saturation up to photocurrents of 30 mA. For type 1 coplanar waveguide devices, the measured millimetre-wave output power at 110 GHz was 10 dBm at a 36 mA photocurrent with a DC responsivity of 0.36 A/W [17].

5. THz heterodyne generation

As described in Section 3 the photodiode was integrated with Bow-Tie and Log-Periodic antennas for broadband emission and a resonant sub-millimetre wave antenna in order to achieve high power over a narrow range of frequencies. A Bow-Tie antenna (Fig. 3b) and a Log-Periodic (Fig. 3c) antenna were designed for optimum operation from 250 GHz and 150 GHz respectively up to 1.5 THz limited by the feed. The resonant antenna was designed for operation around 450 GHz and 900 GHz (Fig. 3d). The magnitude of the radiation resistance of the resonant antenna was designed to be of the order of 100 Ω at the frequencies of operation, for efficient emission. The experimental arrangement used a hemispherical silicon lens for efficient coupling of the THz signal into the power meter. The heterodyne system built for this series of measurements used lasers as selective filters to generate high spectral purity signals from 100 GHz to 1 THz with a Full Width at Half Maximum (FWHM) of <10 Hz. The signal emitted from the antenna was therefore single frequency as determined by the

#126657 - $15.00 USD Received 7 Apr 2010; revised 29 Apr 2010; accepted 29 Apr 2010; published 11 May 2010

heterodyne system. Figure 6 shows the measured extracted power at frequencies ranging from 100 GHz to 1 THz. Figure 6a shows that the response of the type1, resonant antenna integrated devices resulted in two narrowband emission peaks around 450 GHz and 900 GHz. The maximum extracted power was 148 μW at a frequency of 457 GHz and 24 μW at 914 GHz with an input optical power of 100 mW. Preliminary measurements were performed on unpackaged type 2 devices with broadband antennas as well (Fig. 6b). Broadband emission was obtained for frequencies up to 612 GHz with 105 μW at 255 GHz, 30 μW at 408 GHz, 16 μW at 510 GHz and 10 μW at 612 GHz, the last result being at a DC photocurrent of 13 mA, a bias level of −3.5V and an input optical power of only 40 mW. No measurements were performed above 612 GHz because of the limitations imposed by the minimum detectable power of the power meter (5 μW). The ratio of the THz emitted power divided by the square of the optical input power (in W^{-1}) at a certain frequency [18], which can be defined as a figure of merit, ranged from 1 W^{-1} at 110 GHz [17] to 0.053 W^{-1} at 306 GHz and 0.0024 W^{-1} at 914 GHz substantially exceeding previously published results with 0.1 W^{-1} at 100 GHz, 0.001 W^{-1} at 300 GHz and 0.000022 W^{-1} at 1.04 THz [13]. High THz figure of merits have also been reported for GaAs MSM-TW-PDs using pulsed rather than CW excitation [19].

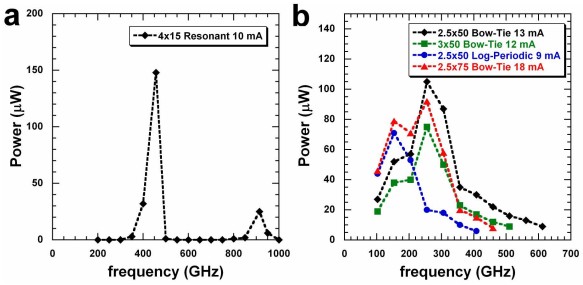

Fig. 6. Emitted THz power as a function of frequency. (a) Narrowband emission from type1, 4x15 μm^2 devices integrated with resonant antennas, (b) Broadband emission up to 612 GHz from type 2 devices (device dimensions in μm^2, antenna type and photocurrent levels given in the inset)

6. Conclusions

This paper presents an efficient ultrafast photodetector that could be used to generate a high purity THz signal, covering frequencies up to 1 THz. The technique relies on the enhanced performance of a waveguide-fed, Traveling-Wave Uni-Traveling Carrier Photodiode. The TW-UTC-PD achieved record levels of continuous wave THz figure of merit up to 612 GHz from broadband antennas and at 457 GHz and 914 GHz with resonant antennas. It is also interesting to note that the power spectral density is far higher than for sources using short pulses and photoconductive antennas as the power is spread over a <10 Hz linewidth. In the future, since the device saturates at relatively high photocurrent (>30 mA), it is anticipated that the OHG Technique implemented with high-bandwidth photodiodes will allow for higher power in the THz domain with an optimised design of the system. It can be further noted that the waveguide-fed configuration can allow for photonic integration with other photonic devices. This would lead towards a fully integrated OHG THz emitter. Finally, it is also expected that the combination of several devices into an array should allow for high output power close to the mW level at 1 THz.

Acknowledgements

This work was supported by the PRINCE (GR/S86631/01) and PORTRAIT (EP/D502233/1) Engineering and Physical Science Research Council grants.

#126657 - $15.00 USD Received 7 Apr 2010; revised 29 Apr 2010; accepted 29 Apr 2010; published 11 May 2010